Coastal Engineering 56 (2009) 285–296

Contents lists available at ScienceDirect

Coastal Engineering

journal homepage: www.elsevier.com/locate/coastaleng

Vorticity and intermittency within the pre-breaking region of spilling breakers

S. Longo *

Department of Civil Engineering, University of Parma, Viale G.P. Usberti, 181/A, 43100 Parma, Italy

ARTICLE INFO

Article history:
Received 25 March 2008
Received in revised form 2 September 2008
Accepted 10 September 2008
Available online 14 October 2008

Keywords:
Waves
Breakers
Turbulence
Vorticity
Wavelets

ABSTRACT

This paper presents measurements and analysis of fluid velocity within the context of spilling waves. The data have been collected using 2-D Laser Doppler Velocimetry in pre-breaking monochromatic waves generated in a wave tank. The analysis is performed using orthogonal wavelets and, in addition to the classical criterion adopted in applying Taylor's hypothesis, a new algorithm is proposed for the eduction of eddies at different length scales. The contribution of different scale vortices is computed, and phase is resolved. Microvortices (smaller than the breaker height but larger than the dissipative vortices) and mid-size vortices (with length ranging from the breaker height to the wave length) carry out most turbulence energy under wave crest. The phase average vorticity and strain rate is computed at different wave lengths, with the analysis of intermittence. The intermittency factor shows spikes in the wave crest, especially for turbulence in small vortices.

1. Introduction

In recent years it has become customary to describe turbulent fields as a mixing of coherent structures of different length scales. Turbulence, instead of a continuum in the flow field, seems to be organised in spatial structures. Without detailing the nature and aspect of a coherent structure, we simply regard it as a recognisable pattern, with a certain degree of determinism. Most of the known coherent structures have a specific capacity for transporting momentum, and hence play important roles in the overall dynamics. Nadaoka et al. (1989) demonstrated that large-scale eddy motion is responsible for the excessive mass flux and enhanced momentum transport in breaking waves. In addition, they demonstrated that vorticity related to large eddies also reduces the wave height favouring the transformation of energy into kinetic energy instead of potential energy.

Our interest in coherent structures in waves is motivated by the important role they play in free surface flows with a movable bottom, as they strongly modify the free surface and affect sediment transport. Coherent structures are intimately related to intermittency, whose pattern is a sequence of intervals of evident strong turbulent fluctuations and intervals of much weaker turbulent fluctuations. Sediment transport in suspension is essentially organised in intermittent events, with sediment being lifted from the bottom and then moved by the mean current. Intermittent events are intimately related to coherent structures.

Many experiments have clearly confirmed the existence of eddies of different length scales in breaking waves (Nadaoka et al. 1989; Chang and Liu, 1998), with large eddies that once generated by the breaking process rotate and assume appearance of oblique vortices. The oblique vortices are the most effective in extracting energy from the mean motion. Lin and Rockwell (1994) studied the evolution of a quasi-steady breaking wave in terms of vorticity. Chang and Liu (1998) studied velocity and vorticity under a breaking wave using Particle Image Velocimetry. Coherent structure and turbulence under breaking waves was experimentally analysed using Digital Particle Image Velocimetry by Melville et al. (2002). Their experiments essentially refer to waves breaking in deep water. As a consequence, many of their results cannot be compared with the results of the present study, but we can learn from their investigation that coherent structures and mean flow generated by breaking waves, and readily identified in the laboratory, may be very difficult to isolate in the field.

The detection of coherent structure relies on an *ad hoc* experimental technique that is often supported by algorithms during data analysis. Large eddies can be easily detected using photographs or visualisation techniques, whilst the smaller eddies can be detected using proper analysis of the velocity signal, as pattern-recognition methods and conditional sampling. In a 2-D perspective a coherent structure is defined as a region with local swirling motion. Techniques used for extracting eddies in a flow field include: (1) a direct analysis of the vorticity field; (2) a Galilean decomposition, which consists in translating the velocity field by an amount equal to the advection velocity of the coherent structure under identification; (3) low-pass filtering the velocity signal in order to remove the small scale contribution; (4) analysis of the velocity gradient tensor; (5) algorithms based on a wavelet transform of the velocity vector field (Camussi, 2002).

Coherent structures are strictly related to intermittency, with a large degree of intermittency expected at all length scales. The concept of intermittency and coherent structures involves considering

* Tel.: +39 0521 905157; fax: +39 0521 905924.
E-mail address: sandro.longo@unipr.it.

0378-3839/$ – see front matter © 2008 Elsevier B.V. All rights reserved.
doi:10.1016/j.coastaleng.2008.09.003

fluid velocity as a composition of a mean-time value, a coherent component and a purely random component. The random component is commonly defined as turbulence. The assumption of (quasi-) determinism is behind the mean-time and the coherent components of the velocity field, and proper modelling is required for the purely random component. Turbulence generation is an intermittent phenomenon, but dissipation also seems to be organised in patches rather than being uniformly present in the flow field. The measurements by George et al. (1994) confirm that dissipation in the surf zone is an intermittent process following a lognormal distribution (Kolgomorov, 1962; Obukhov, 1962). Intermittency on a small scale was reported by Batchelor and Townsend (1949) in experiments designed to study turbulence behind a grid. Another important step forward in analysing intermittence in turbulence is due to Kovasnay et al. (1970), who introduced the intermittency function $I(\mathbf{x},t)$ (equal to 1 for turbulent flow and 0 for non-turbulent flows), which when averaged in time gives the local intermittency factor γ as defined by Townsend (1976). The connection between coherent structures and intermittence is an important aspect of turbulence modelling. Coherent structures generate most of the turbulent shear stress according to many researchers, even in homogeneous turbulence. The main effect of disregarding the presence (or the effects) of these families of eddies is the poor adherence to reality of some common assumptions, with eddy viscosity being expressed as the behaviour of the turbulence stresses in terms of the mean velocity gradients.

Vorticity at the scale of the wave crest and intermittency under waves in the pre-breaking stage are investigated within the present study. The measurement section in the pre-breaking region was selected for convenience with which measurements could be obtained. In the pre-breaking domain the flow field is optically accessible for most of the wave cycle and the breaker does not entrap air bubbles, which frequently un-lock the laser signal. Differences are expected between the breaking and post-breaking sections. A sketch of the spatial distribution of velocity and velocity fluctuations in a spilling breaker is reported in Nadaoka and Kondoh (1982). The differences between the pre-breaking section and the breaking section are limited when considering horizontal velocity (mean and fluctuating), and are more evident with respect to vertical velocity. In our measurement section we expect lower spatial gradients for most of the variables of interest in the breaking or post-breaking section. The difference is much more evident in the immediate post-breaking stage, after crest crossing of the measurement section.

The main aspects focused upon in the present work rely on a wavelet-based algorithm used to decompose the velocity signal obtained by a 2-D Laser Doppler Anemometry (LDA) into contributions at different frequency (wavenumber) and different location on the time axis. The basic motion in a tank is a regular wave motion. The velocity signal is periodic, and turbulence is superimposed with varying intensity and scale structure, depending on the phase.

The present analysis may be considered a progressive step from the analysis reported in Longo (2003), where energy spectra analysis and spatial correlations of fluid velocity are detailed using wavelets, adopting Taylor's hypothesis with the assumption of the celerity of the wave phase as the advection velocity. It is an approximation which is essentially correct near the wave crest.

In the present manuscript the wavelet decomposition tool is used to detail interaction of eddies, intermittency and vorticity. In the first part we (1) make the same assumption on velocity scale in Taylor's hypothesis as in Longo (2003), and obtain intermittency, vorticity and principal values (and axis) of the rate of the deformation tensor. We then (2) use Taylor's hypothesis assuming that the eddies at a specific scale are convected by eddies at larger scales.

The technique of kinematic composition used within this study is novel, and is based on the assumption that vortices of a specific size are convected by vortices of larger size. This assumption belongs to the widely accepted model of energy cascade. The idea that vortices of a specific size are swept along by larger size vortices is not new, and is present in the Richardson phenomenological turbulence approach (Richardson, 1922) and is referenced by Obukhov (1941a,b) and Frisch (1995). The fact that the kinematic of the vortices cannot be neglected in the computation of Taylor's hypothesis based on correlations has been noted previously, as in Loth and Stedl, 1999. Verification of the use of wavelet decomposition in detecting singularities in the velocity time series, and confirmation that these singularities are not merely mathematical artefacts, is reported in Camussi and Gui (1997) and Camussi (2002). We suggest that the conceptual model behind the proposed technique is reliable, and consequently, has been applied to LDV data of the present investigation. We wish to add that further verification using PIV data or the Collective Light Scattering diagnostic (Honoré and Grésillon, 2000) is necessary.

In Section 2 a short description of the experiments is given, with the following section (Section 3) presenting a classical time domain analysis of the results. Data analysis using wavelets is presented in Section 4, with emphasis on a new technique proposed for eduction of coherent structures in a velocity vector field. Analysis of strain rate tensor is presented in Section 5. Section 6 is devoted to intermittency as computed using wavelets in the scale analysis in turbulence fields. Turbulence energy evolution and turbulence analysis near free surface is analysed in Section 7.

2. The experiments

The present analysis refers to experiments on spilling breakers in a wave flume, with Laser Doppler Velocimetry measurements taken in the immediately pre-breaking section. The experiments were carried out in the small flume in the laboratory of the Ocean and Coastal Research Group at the Universidad de Cantabria in Santander, Spain. The flume is 24 m long, 0.58 wide and 0.8 m deep, and has glass side-walls and bottom (Fig. 1).

The wave generator has a paddle with an active absorption system in order to correct for the presence of long waves in the channel. A false Plexiglas bottom was installed in the wave tank, creating a uniform slope 1:20 starting 8.0 m from the paddle. The slope was sealed to the walls of the tank, and the gap between the edges of the slope and the side-walls were filled with a silicone resin.

The local wave height was measured using capacitance wave gauges. A 2-D Laser Doppler Velocimeter was used for velocity measurements. It is a back-scatter, four-beam system with a 6 W ion-argon laser generator refrigerated by water. A 30.00 m optical fibre carries laser beams from an optical system to the measurements location, where it is fixed into a two dimensional programmable transverse system. The Doppler frequency information was elaborated by a counter and stored in a PC. The expected error in velocity measurements is 1% of the velocity range. The test refers to a regular wave (5th order generation) having a period equal to $T=3.0$ s and $H=10$ cm with a still water level (s.w.l.) in front of the paddle equal to 37 cm. The wave breaks as a spilling wave. Velocity measurements were carried out in 21 points in the vertical of a single section at 13.0 m from the paddle in the sloping bottom part of the tank, with a still water level $h=12$ cm. The section of measurements is just before the breaking zone, in order to limit the air bubble content and to also allow LDV measurements in part of the crest. The water was added with TiO_2 tracer which was specifically chosen to improve Ultra-Sounds S/N ratio and not LDA S/N ratio (UltraSounds measurements, description and interpretation are not included in the present paper). The first measurement point is the nearest to the bottom. Other points of measurement are equally spaced at 10 mm points along the vertical. Only 19 of these point measurements were suitable for further analysis, which covers more than half of the crest. The measurements lasted for 300 s at each level (100 wave cycles) with a data rate variable during the wave period because it is related to the number of validated bursts per unit time, which varied. In order to obtain a time

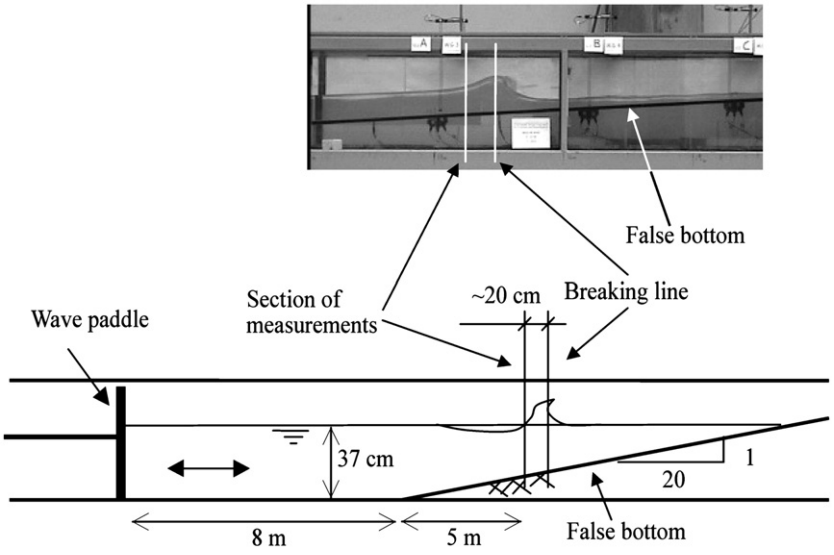

Fig. 1. Layout of the flume.

series with a constant time step, the data have been linearly interpolated at 2 kHz, which is ~20% higher than the mean frequency acquisition data rate. The response of the system is generally satisfactory up to 1.6 kHz. More details on experiments are reported in Longo et al. (2001).

The Iribarren number (Iribarren and Nogales, 1949):

$$Ir = \frac{\tan\alpha}{\sqrt{H_0/L_0}} = 0.59 \tag{2.1}$$

(H_0 and L_0 are the waveheight and the wavelength at the offshore gauge and tanα is the bottom slope) is equal to 0.59. This value is at the upper limit of the spilling breakers and sometimes is also considered in the plunging breakers domain, but the visual impression of the process is that the generated waves break as spilling. Other parameters used to classify breakers do refer to a modified version of the Iribarren number. According to Battjes, 1974, in the breaker zone the surf similarity parameter based on the local wave characteristics but computed on using the offshore values becomes:

$$\xi_b = \frac{1.45\tan\alpha}{(H_0/L_0)^{0.36}} = 0.43 \tag{2.2}$$

The spilling plus bore range is $0.2<\xi_b<0.4$ whereas the plunging plus bore range is $0.4<\xi_b<0.8$.

The expected difference for smaller Iribarren number (i.e. for gently spilling breakers) is related to the global dynamic of the surf zone. On using the parameter (Wang and Yang, 1980):

$$I_b = \frac{1}{2.5\xi_b} \tag{2.3}$$

a general classification for fixed plane beaches describes Flat beaches if $I_b>1$ and Intermediate slope beaches if $0.2<I_b<1.0$. In the present tests results $I_b=0.93$ and the experimental beach is at the upper limit of the Intermediate slope beaches. In order to have an idea of the possible extension of the results for gentler spilling breakers we have to consider the general system that develops at different regimes. Considering Svendsen (1984) separation of the surf zone in Outer surf zone, Inner surf zone and Swash zone, for Flat beaches the three regions are present but a reduced swash zone is expected. The Inner region is dominated by bores and the whole system is stable and tends to filter also a non-linear wave form effects. Also the vertical circulation pattern is developed. For Intermediate slope beaches there is a strong interaction between the breaking wave and the backswash from the preceding wave. The breaker point may be varying because is affected by the amount of reflection. The system is inherently non-linear and potentially unstable.

The results of the present experimental data show a high degree of regularity. The degree of regularity should be enhanced for gentler spilling breakers and the present analysis can be confidently extended to smaller Iribarren numbers.

3. Data analysis in the time domain and relevant scales

The most commonly used average operator in periodic signals is the ensemble or phase average, defined as:

$$\tilde{U}(t) = \frac{1}{N}\sum_{k=0}^{N-1} U(t+kT) \quad 0 \le t < T \tag{3.1}$$

where U is the instantaneous value, N is the number of cycles and T is the period. It is also possible to apply the conditional average, also known as the Variable Interval Time Average (VITA):

$$\tilde{U}(t) = \frac{1}{N}\sum_{k=0}^{N-1} U(t+t_k) \quad 0 \le t < \min(T) \tag{3.2}$$

where t_k is the instant of trigger of the k-cycle, and $\min(T)$ is the minimum time period in the series of N cycles. As the time period of each cycle ($t_k - t_{k-1}$) is not constant (as evidenced in most well-controlled tanks), it is necessary to stretch the data linearly before averaging in order to extend the cycle all over the mean period, with abnormal varying periods also being eliminated in the analysis. Note that the ensemble average distorts and dampens the average in time series in a manner that is not periodic.

A different operator is used if the mass (or any other 'quality' of the data source) is absent during part of the time series:

$$\widehat{U} = \frac{\sum_i \int_{\Delta T_i} U(t)dt}{\sum_i \Delta T_i} \tag{3.3}$$

where ΔT_i are the time steps during water presence. This is known as phasic average.

The VITA technique was used in the analysis of the present data, with the instant of trigger being obtained by performing a moving average of the horizontal velocity signal using $T_m=0.2$ s and selecting the instant of maximum horizontal velocity in the moving averaged

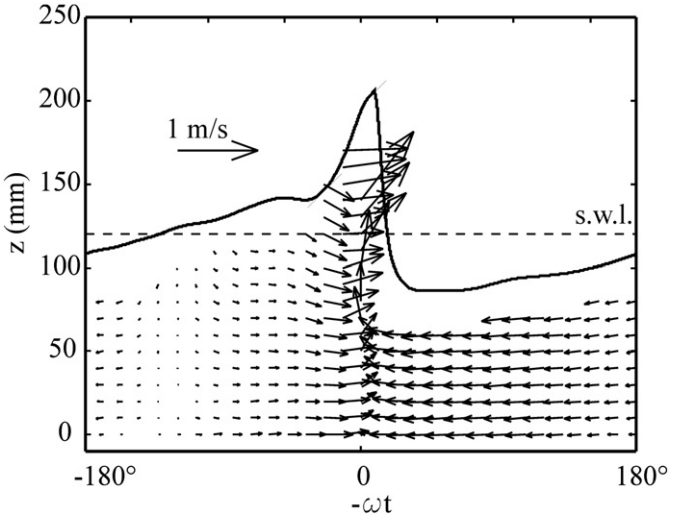

Fig. 2. Phase average velocity.

time series (value of t_k). The resulting periods ($t_k - t_{k-1}$) are very stable and uniform, with a value of $T = 3.0 \pm 0.05$ s for a 95% confidence band. Only those periods in the confidence band were used in computing the phase-averaged horizontal velocity, resulting in ~90% of useful periods. Each time series lasts for 300 s, resulting in ~90 useful periods. The trigger times used for computing the horizontal velocity average were also used for computing the vertical velocity average. Similar computations were carried out to extract the turbulence components. Hereafter the terms phase average stand for VITA.

The phase average velocity is sketched in Fig. 2. The horizontal axis $-\omega t$ may be regarded approximately as kx, where k is the wavenumber.

Turbulence usually involves many scales. A classical interpretation of turbulence is the cascade mechanism (Tennekes and Lumley 1972; Hinze, 1975), with energy contained at large scales (small wavenumber, essentially related to the geometry of the flow field) being transferred to small scales (large wavenumber) where it is turned into heat by viscosity. In the flow field generated by a spilling breaker two important macro-scales are the wave length and the breaker height. The micro scale is essentially Taylor's length micro scale λ_E, and within the context of isotropic turbulence (Batchelor 1982) is related to the rate of dissipation of energy ε:

$$\varepsilon = \frac{15\nu < \widetilde{u'^2} >}{\lambda_E^2} \tag{3.4}$$

u' is the fluctuating component of the fluid velocity and ν is the fluid viscosity. The rate of dissipation, using a dimensional concept, allows the definition of the Kolgomorov length scale of dissipation $\eta_k \equiv (\nu^3/\varepsilon)^{1/4}$, which is evaluated on the assumption that most energy is dissipated by viscosity acting efficiently in dampening microvortices.

Our measurements are in the time domain, with a probe fixed in space whilst collecting a time series of fluid velocity. Most turbulence theories refer to wave number instead of frequency, and a transformation is necessary. The widely used transformation relies on Taylor's approximation, which if we neglect all terms in the balance of momentum other than fluid acceleration, states that:

$$\frac{\partial}{\partial t} \approx -U\frac{\partial}{\partial x} \tag{3.5}$$

where U is a velocity scale, and the other two velocity components, V and W, are been assumed to be negligible, and $u \ll U$, with u representing the scale of turbulence (u/U less than ~0.1 and is more likely to be satisfied at a high wave number, see McComb, 1990). In the present experiments beneath the still water level the phasic average horizontal velocity has a non-dimensional value $\overline{u}/\sqrt{gh} \sim 0.1$ (h is the local still water depth) while the horizontal turbulence intensity has a non-dimensional value (phasic average) $u'/\sqrt{gh} \sim 0.045$ (see Longo, 2003, Figs. 3b and 5b). The ratio is $u/U = 0.45$. Above the still water level the values are $\overline{u}/\sqrt{gh} \sim 0.5\ 0.8$ and $u'/\sqrt{gh} \sim 0.055$; the ratio is $u/U = 0.07 \div 0.11$ and Taylor's hypothesis is better satisfied.

The corresponding transformation is:

$$\frac{f}{U} = \frac{|\mathbf{k}|}{2\pi} = \frac{k}{2\pi} \tag{3.6}$$

where k is the modulus of the wavenumber.

A rough computation, assuming a velocity scale equal to $\sqrt{\kappa}$ (κ is the turbulent kinetic energy) and the computed Taylor's length micro scale equal to ~0.2 mm, gives $k_{max} = k_d = 5 \times 10^3$.

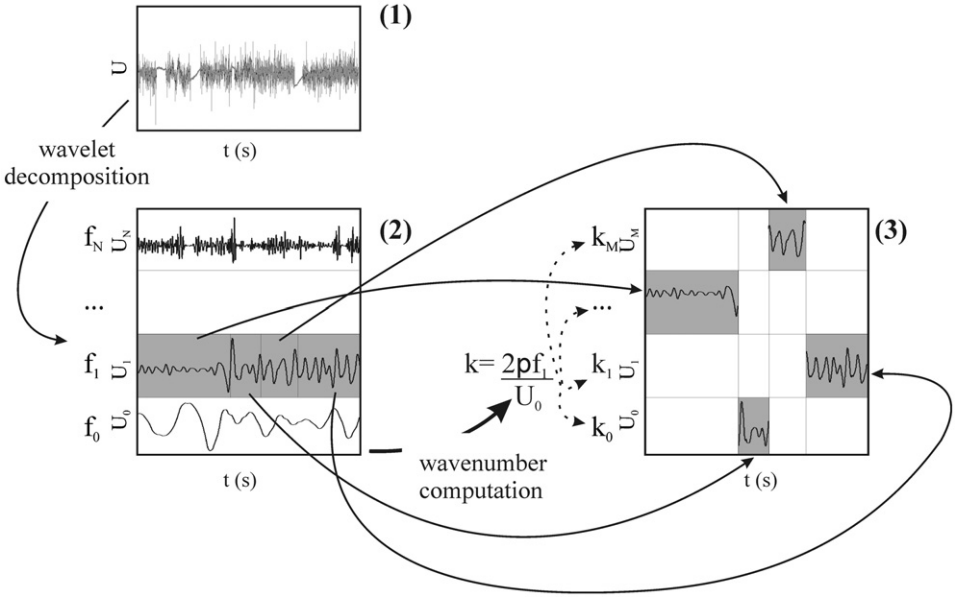

Fig. 3. Process of transformation of the raw signal (panel 1) into wavelet components (panel 2) and into wavenumber vs time components (panel 3).

4. Data analysis using wavelets

4.1. Decomposition in eddies

In order to separate vortices of different size, the first step is computing the wavelet coefficients. The signal is usually divided in power-of-two samples and is projected into the chosen wavelet family using fast numerical algorithms if available. Specific care should be devoted to the method of computation and to the algorithm, which can influence the transform, especially at small scales. We transform the entire length of the signal and then phase average the wavelet coefficients over each wave cycle. At scales larger than the wave period, the average of the wavelet coefficients should allow for the evaluation of possible subharmonic effects. More details on wavelets used are reported in Longo (2003).

Turbulence extracted using the technique described in Section 3 has been decomposed in Daubechies fourth order wavelets. The results are largely (but not completely) independent of the type of wavelet. In general, the choice of the wavelet family should be chosen according to the expected shape of the coherent structures in the flow field. Choosing a different wavelet family can spreads the spectrum between nearby wavelet levels and, if the shape of the wavelet is well far from the shape of the coherent structures present in the flow field, can hide most of the useful information. The length of the analysed sample is 2^{19} points, corresponding to ≅262 s at a 2 kHz sampling rate. The maximum number of scales allowed is $N=16$. The number of wavelet coefficients at each scale decreases for larger scales. The wavelets are localised in time but not in frequency, and the wavelets display a narrow band spectrum rather than a single line spectrum. Their frequency resolution is roughly related to the level j, depending on the shape of the wavelet. The scale is related to level j by $a=2^j$. The higher the level (the scale), the lower the time resolution (and the lower the frequency). At the j-level wavelet the spectrum has significant energy in the range $[f_{acq}2^{-j-1}-f_{acq}2^{-j}]$, where f_{acq} is the frequency of acquisition of the time series. The frequency covered by the decomposition has an upper limit equal to $f_{acq}/2$, and a lower limit equal to $f_{acq}/2^{(N+1)}$. In the present experiments, level 1 covers the frequency range [500, 1000] Hz, and the maximum allowed level covers the frequency range [0.015, 0.03] Hz. Coarser details are included in the approximation A_{16}.

Level 1 wavelets (maximum frequency) are not very representative and always have a negligible energy. This is despite a data rate at 2 kHz being obtained by over-sampling the available data set in an effort to obtain a constant Δt. Additionally, measuring points far from the bottom and near the free surface are associated with a smaller effective data rate due to the presence of strong disturbances. Moreover, using Taylor's hypothesis of frozen turbulence results in a low velocity scale mapping the higher frequency into a very small length scale. But the minimum value of the length scale has to be of the order of the volume of measurements of the laser system, which is less than 1 mm.

Using PIV, velocity information acquired at the same time in several points of the flow field and the identification and extraction of swirling motion associated with coherent structures has been adequately demonstrated using wavelets (see Camussi, 2002). If fluid velocity is measured in a single point as a time series, coherent structures appear as spikes in the frequency domain, with typical frequency being controlled by their advection velocity. A classical criterion is based on Taylor's hypothesis with the transformation of Eq. (3.6) and a velocity scale equal to the celerity of phase of the wave. This criterion is briefly mentioned within this study as AVCP (Advection Velocity equal to the Celerity of Phase of the wave). In the first part of the present analysis we use that criterion; in a second part we use a different criterion.

The technique employed involves mapping the wavelet frequency into 17 wavelet wavenumbers (the choice of the number of wavenumbers is not critical), ranging from ~0.2 to ~10^4 m^{-1} and logarithmically scaled. Wavelet coefficients were computed using the Discrete Wavelets Transform method (DWT; see Longo, 2003). After the transformation of frequency-wavenumber, the mean energy contribution associated to the i-phase in the period was calculated using equation (see Newland, 1993, p.348):

$$\int_0^1 f^2(x)\mathrm{d}x = \overline{f}^2 + \sum_{j,k} w_{jk}^2\left(\frac{1}{2^j}\right) \tag{4.1}$$

while only summing the square coefficients in the i-phase interval. Extending summation to wavenumbers in a limited range, it is possible to evaluate energy associated with eddies in the corresponding length scale.

As already stated, there are several relevant geometric scales in the flow field under investigation. We can assume that the length of the wave identifies the size scale of a periodic macrovortex, filling the system with energy. Wave height near breaking is also an important length scale. We finally assume that the dissipation range is limited by $k=10^{-1}$ k_d as verified on the base of the analysis of the Kolgomorov spectrum with Pao correlation (see Longo, 2003). Hereafter we call macrovortices those vortices with a length scale greater than the length of the wave, $l>4.0$ m; mid-size vortices those in the range 0.10 m$<l<$4.0 m; microvortices those vortices in the range $2\cdot10^{-3}$ m$<l<$0.10 m, and dissipative vortices those in the range $l<2\cdot10^{-3}$ m. This classification is slightly different from the common classification, which recognizes macrovortices, energy-containing vortices and dissipative vortices. The two extreme bands ($l>4.0$ m and $l<2\cdot10^{-3}$ m) are much less reliable than the intermediate bands; the first is limited by the geometry of the flume, the second is limited by the spatial resolution of the measurements.

The transformation has been applied to mean fluid velocity and to turbulence separately, for the vertical and the horizontal components at each height level over the bottom.

4.2. Advection Velocity driven by Larger Vortices (AVLV)

A different criterion for mapping frequency onto wavenumber has also been adopted, assuming that the vortices with a specific length scale are convected by vortices of larger length scale. Mapping relies on Taylor's hypothesis with the transformation of Eq. (3.6) and a velocity scale $U(t)$ due to the eddies of larger size. The velocity scale U is obtained by iteration. The overall process is sketched in Fig. 3 and requires the following steps:

- The wavenumber space is divided into different bands. The maximum value of the wavenumbers is chosen on the basis of the spatial resolution of the measurement system (in our case, it is assumed that the spatial resolution of the LDA corresponds to the maximum size of the volume of measurements, ~1 mm; the minimum length scale which can be computed is roughly less than twice the spatial resolution, i.e. ~2 mm; the minimum wavenumber should be related to the geometry of the flow field.
- The time series of the raw signal (panel 1 in Fig. 3) is decomposed into discrete wavelets and then reconstructed at each level, obtaining a time-frequency matrix with rows containing a time series for the corresponding level of wavelets (frequency) (panel 2 in Fig. 3). The allowable number of levels depends on the wavelet family and on the number of points in the series.
- The frequency at each level (the central frequency of the band corresponding to wavelet at that level) is then transformed into wavenumber using Eq. (3.6), with U computed as the contribution of the sum of lower frequency components.
- The velocity signal at each level (frequency) during time intervals corresponding to a specific wavenumber is cumulated with respect to the corresponding time-wavenumber matrix as derived from the raw signal (panel 3 in Fig. 3).

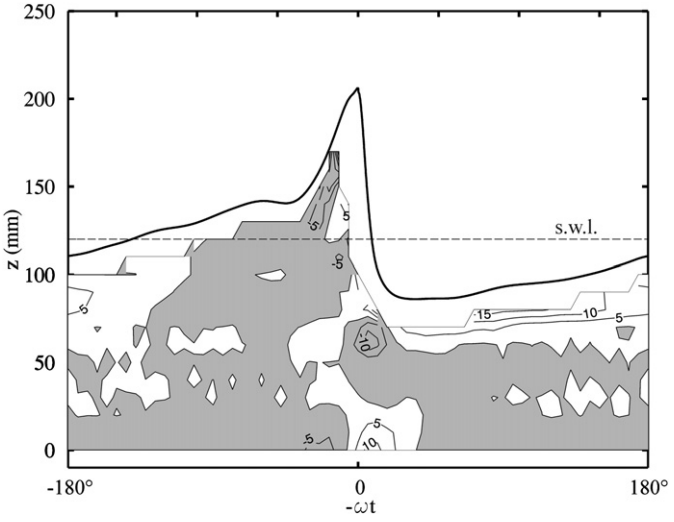

Fig. 4. Phase average turbulence vorticity ω_z. All wave lengths. Clear shadow pattern refers to positive vorticity (counter-clockwise). Contour values in steps of 5 s^{-1}.

- At the end, the time-wavenumber matrix (panel 3) has rows containing time series of velocity, each corresponding to a specific wavenumber band contribution.

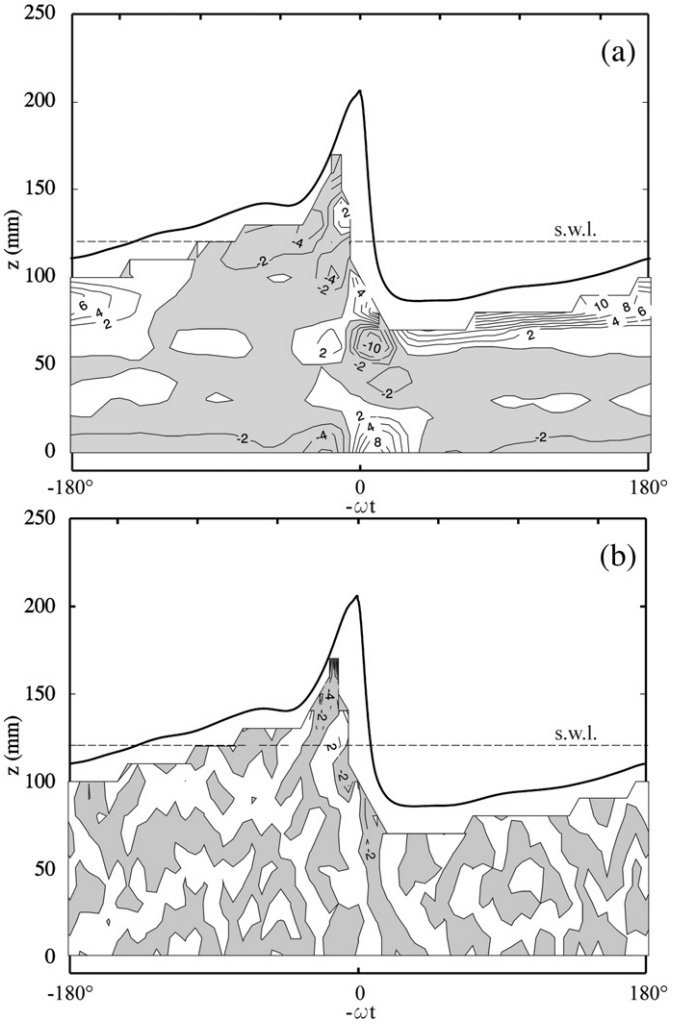

Fig. 5. Phase average turbulence vorticity ω_z contained in eddies with wave length a) l>10 cm; b) 2 mm<l<10 cm; Clear shadow pattern refers to positive vorticity (counter-clockwise). Taylor's hypothesis applied using the celerity of phase of the wave as advection velocity (AVCP). Contour values in steps of 2 s^{-1}.

- In a second and subsequent step the process of transformation is iterated adopting the time series of velocity as stored in the time-wavenumber matrix obtained as the output of the first step.

The convergence is fast and the time-wavenumber matrix (panel 3) does not change after a couple of initial iterations. No space in matrix 3 is

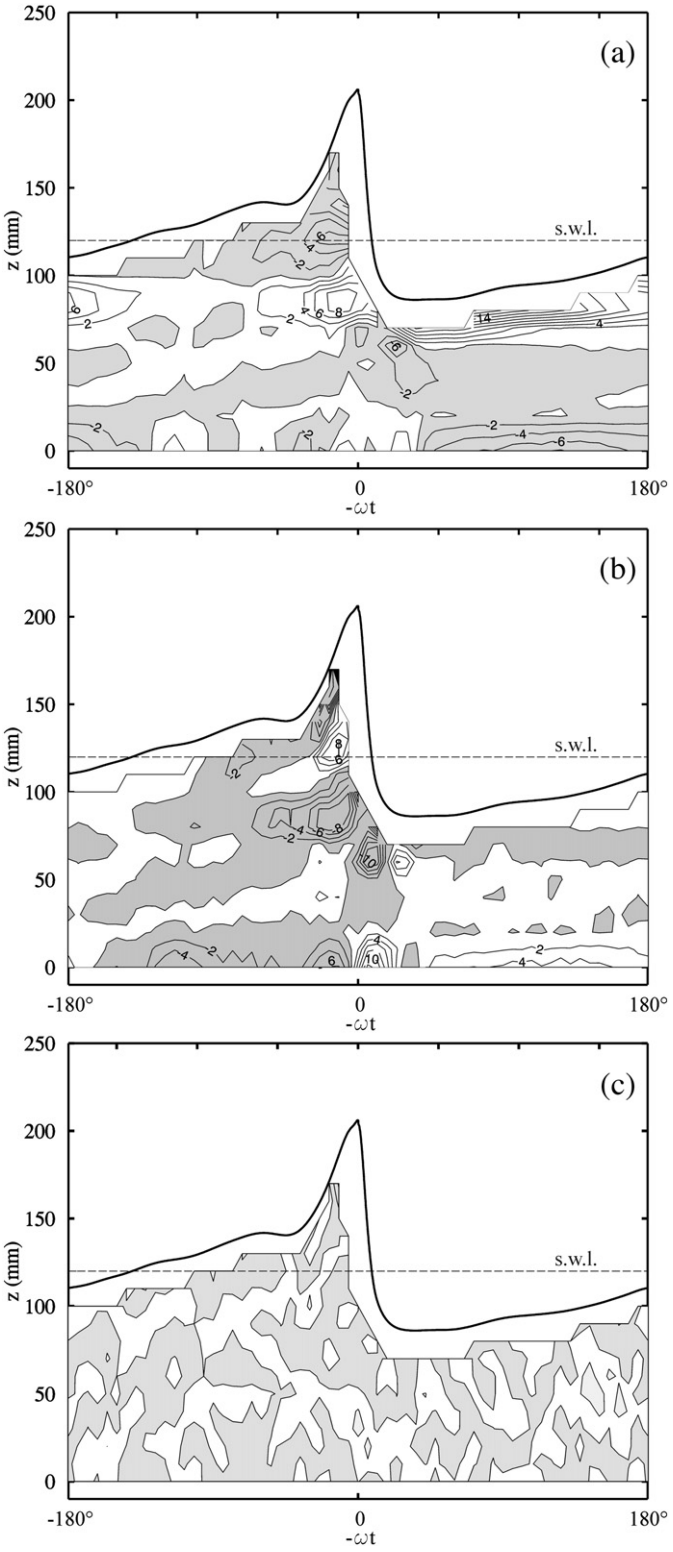

Fig. 6. Phase average turbulence vorticity ω_z contained in eddies with wave length a) l>10 cm; b) 2 mm<l<10 cm; c) l<2 mm. Clear shadow pattern refers to positive vorticity (counter-clockwise). Taylor's hypothesis applied using the larger size vortices induced velocity as advection velocity (AVLV). Contour values in steps of 2 s^{-1}.

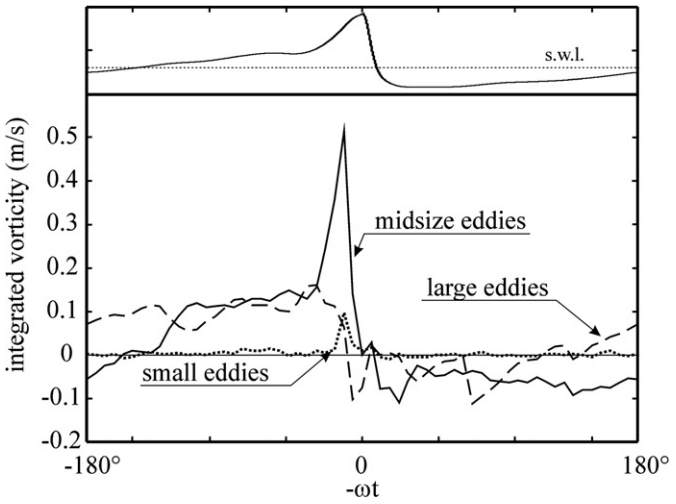

Fig. 7. Integrated vorticity (AVLV criterion for Taylor's hypothesis).

empty if the wavenumber series has been correctly chosen. This is also due to the fact that each row contains the contributions of a band of wavenumbers centred around the nominal wavenumber instead of the contribution of a single nominal wavenumber. Tests with different choices of the wavenumber set show little effect on the results.

The described mapping is partially in the frequency domain (discrete wavelet decomposition takes place in the frequency domain) and partially in the time domains (cumulation process of the velocity field is in the time domain). This criterion is briefly mentioned in this study as AVLV (Advection Velocity driven by Larger Vortices). The results differ from those obtained when adopting a single velocity scale (often the wave celerity) in Eq. (3.5). A single velocity scale compresses eddies with limited advection velocity, and dilates eddies with a strong advection velocity.

The results of the analysis for turbulence are more interesting than similar results for the mean fluid velocity, and will be discussed in more detail.

4.3. Vorticity

The only major sources of vorticity are the breaking free surface and from the bed.

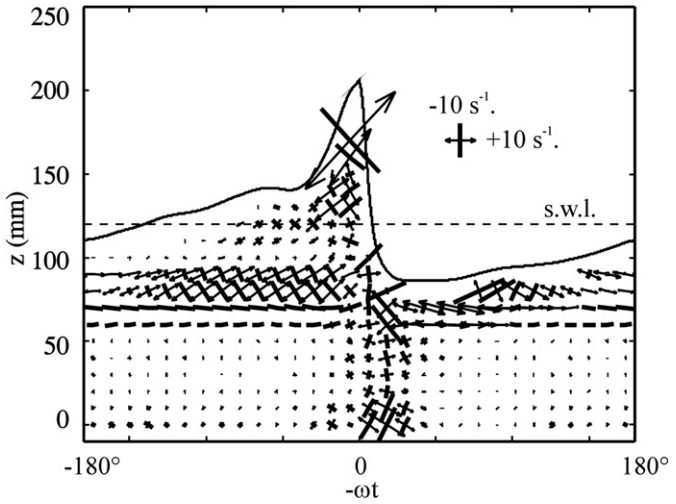

Fig. 8. Phase average principal axes and strain rates. All wave lengths. Arrows refer to stretching; thick segments refer to shrinking.

The phase-averaged component of the turbulent vorticity orthogonal to the plane of motion, defined as

$$\tilde{\omega}_k = \frac{\partial \tilde{u}}{\partial y} - \frac{\partial \tilde{v}}{\partial x} \tag{4.2}$$

has been computed at different wave lengths. The cumulative results representing all wave lengths are plotted in Fig. 4. A clear shadow pattern reflects positive vorticity (counter-clockwise). As long as all wave lengths are included, the computation of vorticity does not depend on the mapping criterion adopted (AVCP or AVLV).

Fig. 5(a, b) depicts the vorticity of different wave lengths computed with the AVCP criterion. The wave lengths chosen for the visualisation of the results correspond roughly to a wavelength higher than the breaker height ($l>10$ cm, Fig. 5a), and smaller than the breaker height (2 mm$<l<$10 cm, Fig. 5b) and a dissipative scale ($l<2$ mm). The contribution of the dissipative scale is very small and has not been reported.

The contribution computed using AVLV for different wave lengths is plotted in Fig. 6(a, b, c).

The patterns of vorticity computed with the application of the AVCP and AVLV mapping criteria are very similar for length scales $l>10$ cm (Figs. 5a and 6a), even though the computed local intensity of vorticity is different. Immediately after breaking a strong vorticity

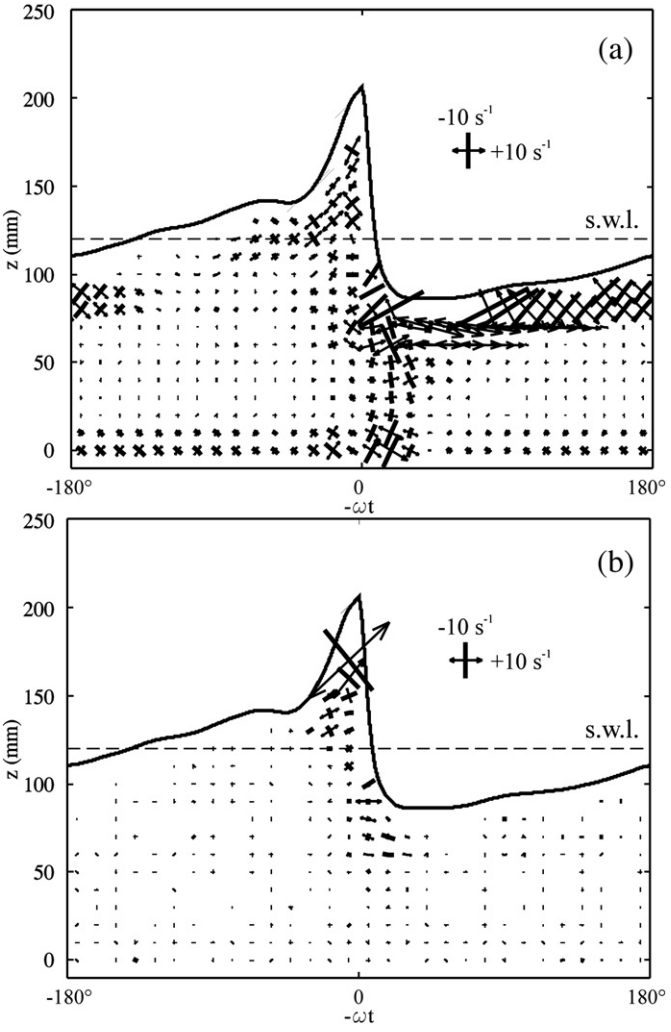

Fig. 9. Phase average principal axes and strain rates. a) $l>10$ cm; b) 2 mm$<l<$10 cm. Arrows refer to stretching; thick segments refer to shrinking. Taylor's hypothesis applied using the celerity of wave as advection velocity (AVCP).

(positive vorticity in the adopted reference system) fills the system with energy. Then the vortex deepens and diffuses. Deepening is quite fast immediately after breaking, and is slower on subsequent occasions. In the phase interval −150°–0° the convective velocity is from left to right. At ~ −150° the convective velocity is near zero and turbulent vorticity diffusion dominates. After flow reversal, near the free surface new positive vorticity generates and fills the surface layer. At the toe of the breaker a strong vortex develops, which is essentially confined. The source of this vorticity is essentially a fluid deceleration, as computed by Dabiri and Gharib (1997) (hereafter DG). However DG verified that the vorticity is also convected due to the sharp velocity gradient of the fluid near the free surface with respect to the fluid below. Present measurements are not exactly at the free surface, and no sharp velocity gradient is observed at the toe of the breaker (see Fig. 2).

Much stronger is positive vorticity (counter-clockwise), which fills most of the fluid domain near the free surface after breaking and most of the fluid domain near the bottom after flow reversal. These observations are substantially consistent with the measurements of DG, with some differences due to the specific kind of breaking generation they used (pressure drop through honeycomb/screen section of a stream).

Vorticity related to large vortices (Fig. 6a) shows more clearly that at the toe of the breaker negative vorticity is generated and convected,

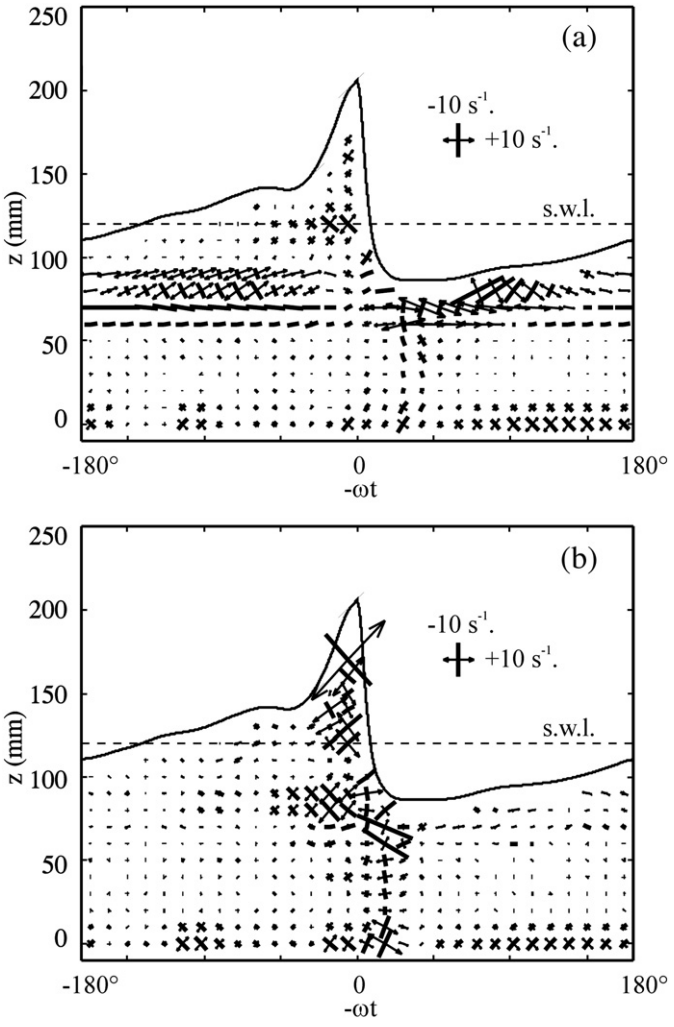

Fig. 10. Phase average principal axes and strain rates. a) $l>10$ cm; b) 2 mm$<l<$10 cm. Arrows refer to stretching; thick segments refer to shrinking. Taylor's hypothesis applied using the larger size vortices induced velocity as advection velocity (AVLV).

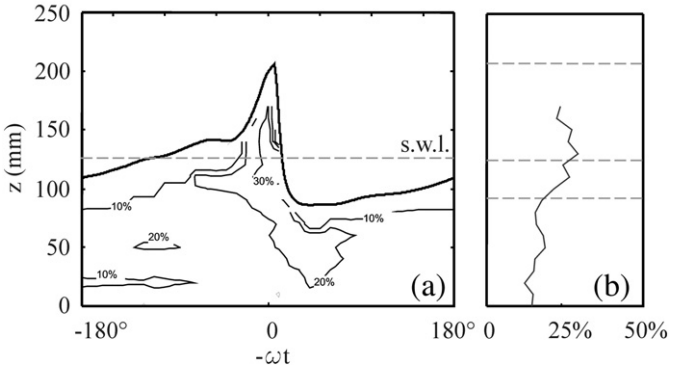

Fig. 11. (a) Intermittency factor for eddies with length scale $l>10$ cm; (b) phasic average in the vertical. Taylor's hypothesis applied using the larger size vortices induced velocity as advection velocity (AVLV).

whereas in the wave crest positive vorticity develops. Smaller turbulent eddies (Fig. 6b) are counter rotating with respect to larger eddies. The similarity between the two families of eddies is high at the toe of the breaker and in the crest, but is poor in most of the fluid flow field. The vorticity at smaller and dissipative scales is more uniform, and no specific pattern is recognizable in Fig. 6c. The pattern of vorticity in AVCP for smaller turbulent eddies (2 mm$<l<$10 cm, Fig. 5b) is more uniform and of smaller magnitude than in AVLV (Fig. 6b), and seems similar to vorticity in a dissipative scale range ($l<2$ mm) as reconstructed using AVLV (Fig. 6c). The AVLV mapping criterion shifts vorticity towards smaller wavelengths (larger vortices) in comparison to the AVCP mapping criterion, presumably as a consequence of the intrinsic non-linearity of the transformation in Eq. (3.6). In fact, the opposite effect should arise if adopting the transformation in Eq. (3.6) in a linear fashion which considers each wavelength band as non-interacting with the nearby wavelength bands, because the celerity of phase of the wave is larger than the fluid velocity in most of the flow field.

In order to clarify the effect of eddies of different size, vorticity as computed with the AVLV criterion and integrated in the vertical is shown in Fig. 7.

The most important contribution in the crest is due to mid-size vortices, which are faster growing than the larger eddies. Observing the lag of vorticity in large eddies, it can be inferred that larger eddies are partially filled by mid-size eddies, inverting the cascade mechanism. The macrovortices are evidently limited by geometry in the wave crest. It is not possible to balance all the terms in the vorticity equation, because vortex stretching, which is well-known to be the most important mechanism in energy transfer in turbulence, is not represented in 2-D analysis.

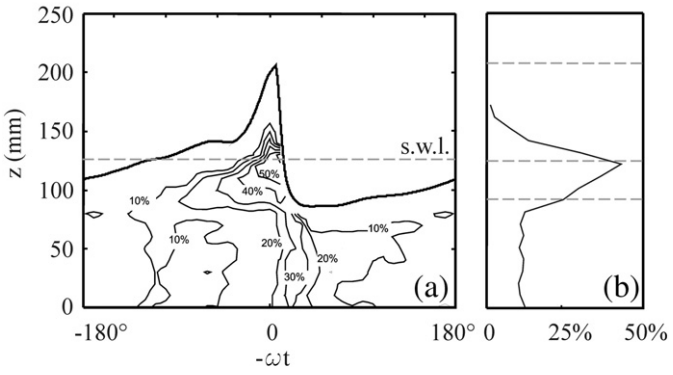

Fig. 12. (a) Intermittency factor for eddies with length scale $l=1$–10 cm; (b) phasic average in the vertical. Taylor's hypothesis applied using the larger size vortices induced velocity as advection velocity (AVLV).

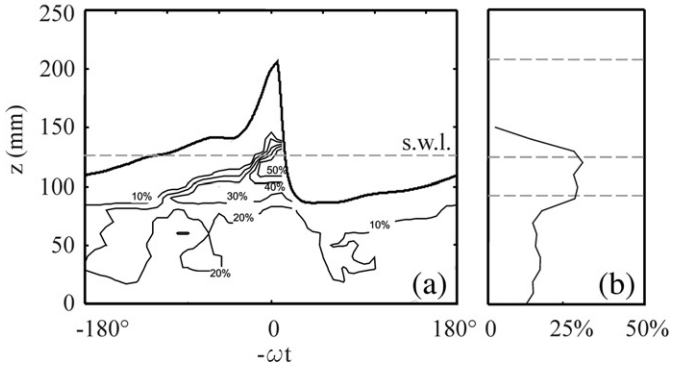

Fig. 13. (a) Intermittency factor for eddies with length scale $l<1$ cm; (b) phasic average in the vertical. Taylor's hypothesis applied using the larger size vortices induced velocity as advection velocity (AVLV).

It is interesting to note that some of the breaking vorticity spreads seaward of the breaking point, and it is an unexpected results. It could be addressed to some waves breaking earlier, but the extreme repeatability of the wave generation guarantees that it is not the case.

Near the bed, the most intense spread of vorticity is where the mean flow at the bed changes sign and eject the flow into the body of water.

5. Principal axes and strain rate

The principal values of the rate of deformation tensor represent the rate of stretching in the principal directions. Principal values are the eigenvalues of the rate of deformation tensor, which in 2-D is represented by:

$$\begin{bmatrix} 2\frac{\partial \tilde{u}}{\partial x} & \frac{\partial \tilde{v}}{\partial x}+\frac{\partial \tilde{u}}{\partial y} \\ \frac{\partial \tilde{v}}{\partial x}+\frac{\partial \tilde{u}}{\partial y} & 2\frac{\partial \tilde{v}}{\partial y} \end{bmatrix} \tag{5.1}$$

and principal directions are the corresponding eigenvectors.

The results are shown in Fig. 8 for all wave lengths. The arrows represent maximum stretching and are proportional to the principal strain rate. The thick segments represent compression (shrinking), which is also proportional to the corresponding strain rate. The principal directions are orthogonal, even though in the plots they appear to be otherwise due to the different scales used for the horizontal and vertical directions. The presence of a uniform shear layer below the wave trough is almost evident, with the principal axes being 45° relative to the stream. The stretching increases strongly in the wave crest and remains at 45°. An important modification of the flow depends on the variation of the strain across the flow. After breaking, the obliquely descendant eddies are essentially stretched with an optimal energy transfer to smaller eddies. Such a mechanism was also experimentally tested and verified by Nadaoka et al. (1989). Computations using the AVCP criterion are plotted in Fig. 9(a, b), and those utilizing the AVLV criterion are plotted in Fig. 10(a, b). The role of larger eddies ($l>10$ cm) in strain rate is shown in Fig. 10a. Larger eddies are responsible for the uniform shear layer below the wave trough being almost horizontal, and also control most of the fluid deformation before breaking near the free surface. Here the principal directions are still at 45°, but shrinking and stretching are inverted relative to post-breaking conditions.

The contribution of smaller eddies (2 mm$<l<$10 cm, see Fig. 10b) is dominant at the toe of the breaker and in the wave crest. Near the bottom larger eddies and smaller eddies generate similar, but opposite, strain rates, which in fact are negligible if considering the contribution made by all eddies.

The principal directions and the polarity of the eigenvalues of the rate of the deformation tensor are almost coincident when comparing AVCP and AVLV data, even though the total strain rate is shared in a different proportion between larger eddies ($l>10$ cm) and smaller eddies (2 mm$<l<$10 cm).

6. Intermittency and coherent structures

Existence of coherent structures in most physical flow fields is widely documented. The coherent structures have been observed in boundary layers (e.g. Elder, 1960), pipes of round cross-section (Wygnanski and Champagne, 1973), and in many other flows. A categorization into 'spots', 'slugs' and 'puffs' was proposed according to some specific properties of the different coherent structures. A free-surface intermittency and a fine-structure intermittency have been often detected. The fine-structure intermittency is particularly interesting because it has

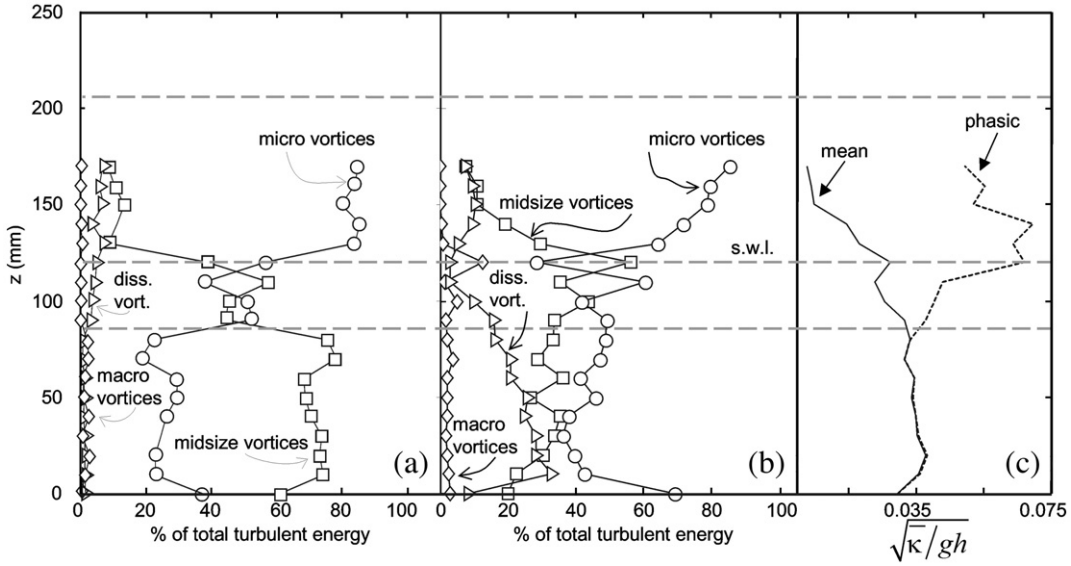

Fig. 14. Energy of different sizes vortices: panel (a) refers to the results obtained adopting AVLV criterion; panel (b) and panel (c) (also presented in Longo, 2003) refers to the results obtained adopting AVCP and to non-dimensional turbulence energy at all scales in the vertical.

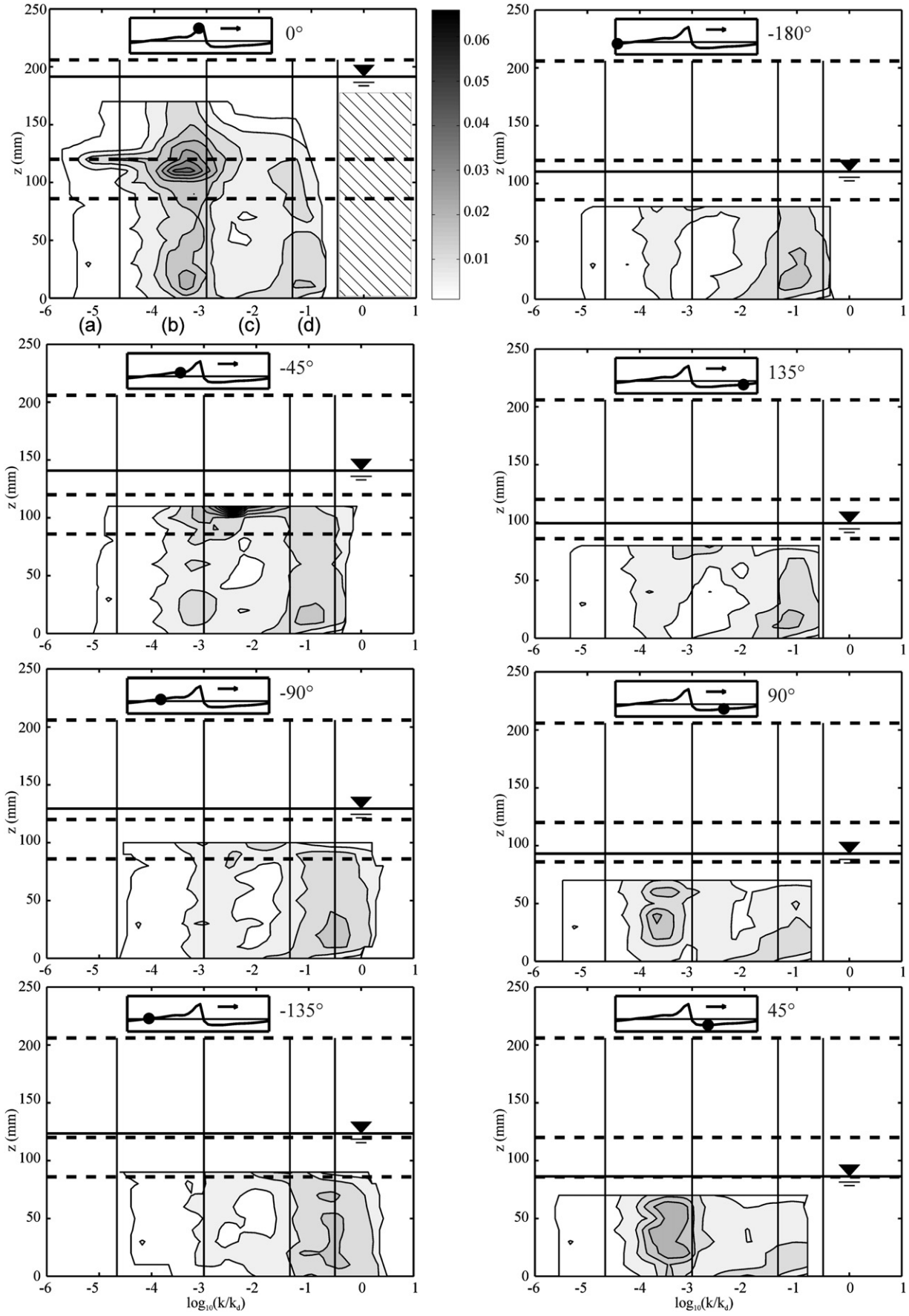

Fig. 15. Turbulence velocity scale $\sqrt{\kappa}$ each 45°. Contour lines each 0.01 m/s. The four wavenumber bands correspond to (a) macrovortices, (b) mid-size vortices, (c) microvortices, (d) dissipative vortices. The dashed area in the upper left panel corresponds to measurement volume size. AVLV criterion for Taylor's hypothesis.

important implications for energy cascading. Kolgomorov (1941) obtained the p-order velocity structure function:

$$\langle \Delta V(r)^p \rangle = \langle [V(x+r)-V(x)]^p \rangle \sim r^{\varsigma(p)} \tag{6.1}$$

where r is the separation scale and $\varsigma(p)=p/3$. On this basis the well-known expression $E(k) \propto k^{-5/3}$ is obtained for the energy spectrum. Several researchers have demonstrated that as a result of intermittency the Kolgomorov scaling law is not completely correct, and that a signature of intermittency is the non-linear dependence of $\varsigma(p)$ on p (Camussi and Gui, 1997). In other terms, the probability distribution function of the velocity difference tends to be non-Gaussian as the separation scale (r) becomes smaller.

More interesting is the fact that Holschneider (1988) and Camussi and Gui (1997) have shown that wavelet coefficients $w(r,x)$ scale as the velocity difference, hence:

$$\langle \Delta V(r)^p \rangle = \langle [V(x+r)-V(x)]^p \rangle \sim w(r,x)^p \tag{6.2}$$

This result strongly favours data analysis using wavelets, because wavelet coefficients are the natural space for analysing the velocity structure function. A suitable method of representing intermittency is the Local Intermittency Measure (LIM) (Farge, 1992), defined as:

$$l(r,x) = \frac{w(r,x)^2}{\langle w(r,x)^2 \rangle_x} \tag{6.3}$$

Computation of LIM has been carried out for eddies of different length scale using the AVCP and AVLV criteria. The results are plotted in Figs. 11, 12 and 13 only for AVLV.

Intermittency assumes higher values in the crest for the smaller eddies (Figs. 12 and 13) and is almost uniform in the vertical for larger eddies (Fig. 11). Higher intermittency is obtained for mid-size eddies near the toe of the breaker. The values are comparable to values obtained by other researchers for different classical turbulent flow fields. There are minor differences in results between the AVCP and AVLV methodologies, being mostly in the wave trough, and confirm that intermittency is a characteristic of the entire spectrum.

The contour lines of the intermittency factor are consistent with a qualitative description of the transfer of vorticity as given by Townsend (1976 p. 232). According to Townsend, vorticity spreads with a bounding surface made of crests and troughs. Viscous diffusion, due to very small eddies, is enhanced by stretching and shrinking induced by larger eddies. The most effective coupling occurs between eddies of comparable size. The transfer process is interrupted if a specific size of eddies is missing. In such a case the bounding surface is merely distorted, but not diffused. In this last situation the effects of an intermittency factor are large. In the present experiments the strongest intermittency is observed in the wave crest, where the fast generation of vorticity at mid-size scale (essentially the breaker height) is not readily followed by diffusion of the bounding surface because of the lack of eddies with a slightly larger size. A similar situation can be observed during flow reversal near 0° for mid-size eddies (Fig. 13).

7. Turbulence energy

Turbulence energy distribution in the vertical as computed with AVCP and AVLV criteria is shown in Fig. 14. The AVCP results were also presented in Longo (2003).

The difference in the crest is not so evident due to the fact that the velocity scale in Taylor's mapping is approximately equal when adopting either criterion. The adoption of the AVLV criterion involves less energy being attributed to dissipative vortices, and the difference between microvortices and mid-size vortices is enhanced below the wave trough. Microvortices contain most of turbulent energy in the crest of both analyses.

Turbulence energy computed adopting only AVLV criterion is presented in Fig. 15 as function of phase and length scale. Frames refer to different phases, each 45° and starting from the immediate post-breaking point (left upper panel). Contour lines refer to turbulence velocity scale vs. water level and wave number (abscissa). The four main wave number bands correspond to: (a) macrovortices, (b) mid-size vortices, (c) microvortices, (d) dissipative vortices. The dashed area refers to a limited space-resolution (due to the finite size of the measurement volume of LDA) or limited time resolution (due to the limited frequency of acquisition). Turbulence energy is high in the immediate post-breaking position, with significant contributions by the mid-size vortices (see left upper panel in Fig. 15). A secondary turbulence energy generation is also evident after flow reversal, and is progressively enhanced in the immediate pre-breaking point. A core of dissipation is always present below the wave trough. 1-D turbulence energy spectra and longitudinal and transverse correlation functions can be efficiently used to detail turbulence evolution. This analysis has been reported in another paper (Longo, 2003).

8. Conclusion

Turbulence and vorticity in immediate pre-breaking and spilling points of laboratory waves has been analysed using wavelet decomposition. In the section from which measurements were obtained, the results differ slightly from those expected in the breaking section, and are significantly different from the results expected in the post-breaking sections (see Nadaoka and Kondoh, 1982, for the spatial distribution of mean velocity and velocity fluctuation).

The energy contribution of different eddy wavenumbers at different phases during the wave cycle has been computed. Mapping from frequency space to wavenumber space is based on Taylor's frozen turbulence hypothesis, and was applied using two different criteria: (a) the advection velocity is equal to the celerity of phase of the wave (AVCP); (b) the advection velocity is equal to the velocity due to larger eddies (AVLV). The AVLV technique is novel, even though it is based on well-established tools like discrete wavelet decomposition and the vortices interaction model adopted for the energy cascade assessment. In comparison to previous studies, the present measurements analyse in detail the structure of the flow field with a specific emphasis on intermittency and flow field characteristics as shared by vortices of different size.

The vorticity computed at different wave lengths shows that eddies of size comparable to breaker height and eddies of size comparable to wave length are rotating in opposite directions in most of the flow field.

Larger eddies are responsible for the uniform shear layer below the wave trough, which is almost horizontal, and also control most of the fluid deformation before breaking near the free surface. Here the principal directions are still at 45°, but shrinking and stretching are inverted relative to post-breaking condition. Smaller eddies control the strain rate at the toe of the breaker and in the wave crest. Near the bottom larger eddies and smaller eddies generate similar, but opposite, strain rates. Near the bottom the strain rate due to these two families of eddies is almost balanced. Notably some of the breaking vorticity spreads seaward of the breaking point, which is unexpected.

Intermittency, defined at different length scales using the Local Intermittency Measure, has been computed using the natural bases offered by wavelet coefficients. The computed intermittency rate reflects the dynamics of the vorticity and the exchange of vorticity at different scales (vortex stretching is not included because the analysis is 2-D and no information is available for span-wise velocity and turbulence).

Acknowledgements

This work is undertaken as part of the Italy–Spain Co-operation Project 1999–2000, funded by MURST of Italy and of Spain. I wish to

express many thanks to the technicians and to the staff of the Ocean and Coastal Research Group Laboratory, in Santander (Spain), for their valuable collaboration in carrying out experiments. It has also been partly supported by MAST III–SASME Project ("Surf and Swash Zone Mechanics") founded by the Commission of the European Communities, Directorate General Research and Development under contract no. MAS3-CT97-0081.

References

Batchelor, G.K., 1982. The Theory of Homogeneous Turbulence. Cambridge Univ. Press, Cambridge, UK. pp. 197+xi, ISBN 0-521-04117-1.
Batchelor, G.K., Townsend, A.A., 1949. The nature of turbulent fluid motion at large wavenumbers. Proc. R. Soc. Lond., A 199, 238–255.
Battjes, J.A., 1974. Surf similarity. Proc. 14th Int. Conf. Coastal Eng. ASCE, pp. 1419–1438.
Camussi, R., 2002. Coherent structure identification from wavelet analysis of particle image velocimetry data. Exp. Fluids 32, 76–87.
Camussi, R., Gui, G., 1997. Orthonormal wavelet decomposition of turbulent flows: intermittency and coherent structures. J. Fluid Mech. 348, 177–199.
Chang, K.-A., Liu, P.L.-F., 1998. Velocity, acceleration and vorticity under a breaking wave. Phys. Fluids 10, 327–329.
Dabiri, D., Gharib, M., 1997. Experimental investigation of the vorticity generation within a spilling water wave. J. Fluid Mech. 330, 113–139.
Elder, J.W., 1960. The flow past a flat plate of finite width. J. Fluid Mech. 9, 133–153.
Farge, M., 1992. Wavelet transforms and their applications to turbulence. Ann. Rev. Fluid Mech. 24, 395–457.
Frisch, U., 1995. Turbulence. The Legacy of A. N. Kolgomorov. Cambridge University Press, Cambridge.
George, R., Flick, R.E., Guza, R.T., 1994. Observation of turbulence in the surf zone. J. Geophys. Res. 99 (C1), 801–810.
Hinze, J.O., 1975. Turbulence. McGraw-Hill series in mechanical engineering, New York. pp.790 + x, ISBN 0-07-029037-7.
Holschneider, M., 1988. On the wavelet transformation of fractal object. J. Stat. Phys. 50, 953–993.
Honoré, C., Grésillon, D., 2000. Turbulence cascade and dynamical exchange between spatial scales. J. Fluid Mech. 411, 187–211.
Iribarren, C.R., Nogales, C., 1949. Protection des ports. Sect. 2. comm. 4, 17th Int. Nav. Cong., Lisbon, pp. 31–80.
Kolgomorov, A.N., 1941. Dissipation of energy in the locally isotropic turbulence. In: Friedlander, S.K., Topper, L. (Eds.), Turbulence, Classic papers on statistical theory. Interscience, pp. 151–161.
Kolgomorov, A.N., 1962. A refinement of previous hypotheses concerning the local structure in a viscous incompressible fluid at high Reynolds number. J. Fluid Mech. 13, 82–85.
Kovasnay, L.S.G., Kibens, V., Blackwelder, R., 1970. Large scale motion in the intermittent region of a turbulent boundary layer. J. Fluid Mech. 41, 283–325.
Lin, J.-C., Rockwell, D., 1994. Instantaneous structure of a breaking wave. Phys. Fluids 6 (9), 2877–2879.
Longo, S., 2003. Turbulence under spilling breakers using discrete wavelets. Exp. Fluids 34, 181–191.
Longo, S., Losada, I.J., Petti, M., Pasotti, N. & Lara, J. 2001 Measurements of breaking waves and bores through a USD velocity profiler. Technical Report UPR/UCa_01_2001, University of Parma, University of Santander.
Loth, E., Stedl, J., 1999. Taylor and Lagrange correlations in a turbulent free shear layer. Exp. Fluids 26, 1–6.
McComb, W.D., 1990. The Physics of Fluid Turbulence. Oxford University Press, Oxford, UK. pp. 572 + xxiv, ISBN 0-19-856256-X.
Melville, W.K., Veron, F., White, C.J., 2002. The velocity field under breaking waves: coherent structures and turbulence. J. Fluid Mech. 454, 203–233.
Nadaoka, K., Kondoh, T., 1982. Laboratory measurements of velocity field structure in the surf zone by LDV. Coast. Eng. Jpn. 25, 125–145.
Nadaoka, K., Hino, M., Koyano, Y., 1989. Structure of the turbulent flow field under breaking waves in the surf zone. J. Fluid Mech. 204, 359–387.
Newland, D.E., 1993. Random Vibrations, Spectral Analysis & Wavelet Analysis, 3rd Ed. Prentice Hall, Singapore. xxix + 477 pp., ISBN 0-582-21584-6.
Obukhov, A.M., 1941a. On the distribution of energy in the spectrum of turbulent flow. Dokl. Akad. Nauk SSR 32 (1), 22–24.
Obukhov, A.M., 1941b. Spectral energy distribution in a turbulent flow. Dokl. Akad. Nauk SSR Ser. Geogr. Geofiz. 5 (4–5), 453–466.
Obukhov, A.M., 1962. Some specific features of atmospheric turbulence. J. Fluid Mech. 13, 77–81.
Richardson, L.F., 1922. Weather Prediction by Numerical Process. Cambridge University Press, Cambridge.
Svendsen, I.A., 1984. Wave heights and set-up in a surf zone. Coast. Eng. 9, 151–181.
Tennekes, H., Lumley, J.L., 1972. A First Course in Turbulence. The MIT Press, Cambridge, MA. pp. 300 + xii, ISBN 0-262-20019-8.
Townsend, A.A., 1976. The Structure of Turbulent Shear Flow. Cambridge Univ. Press, Cambridge, UK. pp. 429 + xi, ISBN 0-521-29819-9.
Wang, H., Yang, W.-C., 1980. A similarity model in the surf zone. Proc. 17th Coastal Eng. Conf. ASCE, Sydney, vol. 1, pp. 529–546. Ch. 33.
Wygnanski, I.J., Champagne, F.H., 1973. On transition in a pipe. Part I. The origin of puffs and slugs and the flow in a turbulent slug. J. Fluid Mech. 59, 281–335.